Oliveira, J.P.; Duarte, J.F.; Inacio, P.; Schell, N.; Miranda, R.M.; Santos, T.G.:
Production of Al/NiTi composites by friction stir welding assisted by electrical current
In: Materials and Design (2016) Elsevier

DOI: 10.1016/j.matdes.2016.10.038

Production of Al/NiTi composites by Friction Stir Welding assisted by electrical current

J. P. Oliveira[1, *], J. F. Duarte [1], Patrick Inácio [2], N. Schell [3], R. M. Miranda [2], Telmo G. Santos [2]

[1] CENIMAT/i3N, Faculdade de Ciências e Tecnologia, Universidade Nova de Lisboa, Portugal

[2] UNIDEMI, Departamento de Engenharia Mecânica e Industrial, Faculdade de Ciências e Tecnologia, Universidade Nova de Lisboa, 2829-516 Caparica, Portugal

[3] Institute of Materials Research, Helmholtz-Zentrum Geesthacht, Max-Planck-Str. 1, D-21502 Geesthacht, Germany

* jp.oliveira@campus.fct.unl.pt, corresponding author

Highlights

- Friction stir welding assisted by electrical current was used to produce Al/NiTi/Al composites.

- Use of electrical current facilitates the material flow improving joining.

- The mechanical properties of the composites improved significantly with hybrid process.

- Synchrotron X-ray diffraction was used to identify the microstructural induced changes.

Graphical Abstract

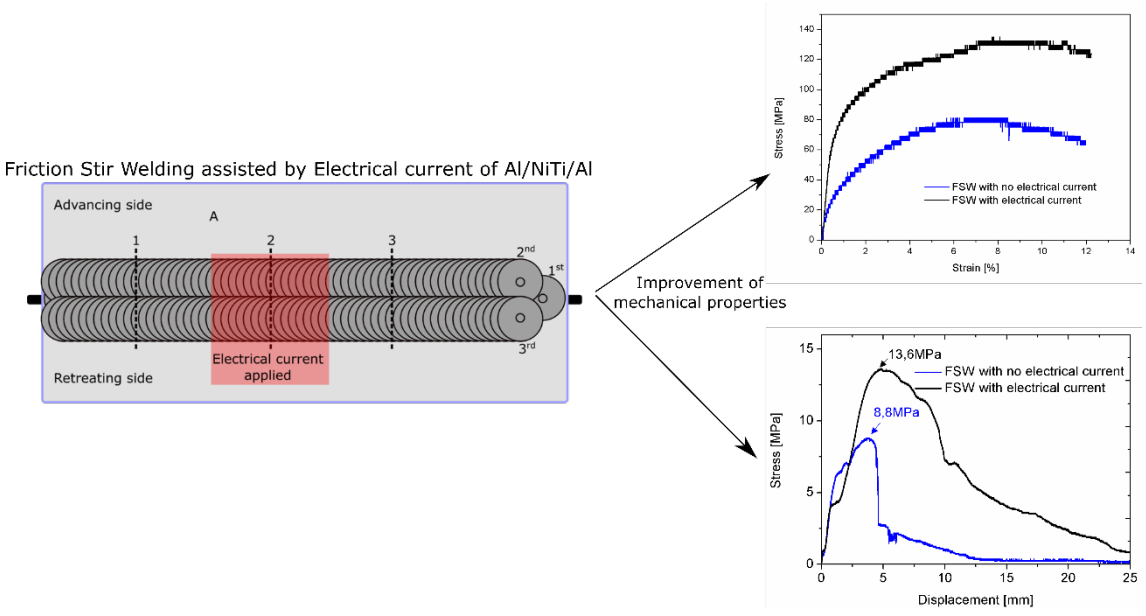

Abstract:

Composite Al structures reinforced with NiTi have been produced by solid-state joining processes in order to prevent brittle intermetallics to form. For this, friction stir welding (FSW) was used in both the conventional and the hybrid variant assisted by electrical current. The hybrid process allows for a better bonding along the NiTi/Al interface since the material viscoplasticity promoted by the higher temperatures achieved during the process facilitates the material flow around the reinforcement. Mechanical characterization of the composites showed that upon bending and pull-out tests, the composites produced by FSW assisted by

electrical current have increasing mechanical properties. Microstructural characterization using synchrotron X-ray diffraction, revealed that composites produced with the hybrid process exhibited a different transformation temperature of the NiTi reinforcements. The fully austenitic NiTi presented both martensite and austenite at room temperature after processing, which can be taken as an advantage for applications where damping capacity of the shape memory alloy are required. The ability to successfully join NiTi to Al may open new structural applications based on these composites.

Keywords: NiTi; Aluminium; Composite structures; Electrical current assisted FSW; Damping.

Introduction

The demand for structural materials that exhibit high damping capacity, superior mechanical specific strength and low density for industrial applications has increased significantly in the past years [1]. However, materials that comply with these requirements are scarce as these properties are often incompatible in metallic alloys [2]. So, research is being developed in new hybrid materials for components that require these characteristics [3].

NiTi shape memory alloys are excellent damping materials [4,5] and present superelasticity and shape memory effect [6, 7]. Both properties are dependent on a reversible austenite ↔ martensite transformation, which can be stress (for the superelastic effect) or temperature-induced (for the shape memory effect) [8].

In order to overcome the aforementioned industrial needs, integration of NiTi with other lightweight materials, such as aluminium, would be beneficial. Such integration could be better performed by joining processes, due to facility in production. However, though NiTi can be easily joined to itself by fusion-based processes [9,10], that is not often the case when dissimilar combinations are required [11,12]. In dissimilar joining involving NiTi by fusion-based techniques, the formation of undesirable brittle intermetallics, is detrimental to the mechanical behaviour of the structure. This can be surpassed by using solid-state processes, such as Friction Stir Welding (FSW) [13]. Some advantages of this technology include high performance joints in difficult to weld materials with almost no distortions and residual stresses, low production costs, since it is low energy consumption and there is almost no need for consumables, and it is an environmentally clean process [14].

From the above mentioned advantages, FSW has been used to produce aluminium matrix-based composites [14,15]. The use of aluminium as a matrix allows good thermal and electrical conductivities and low thermal expansion coefficient and density. Dissimilar joints can be produced using this process with no concerns on possible composition compatibility, which is of great importance to avoid cracking upon solidification as in fusion-based processes.

Recently, a variant of FSW was developed by Santos et al. [16] in which FSW was assisted by electrical Joule effect aiming to increase the material viscoplasticity, thus minimizing and/or eliminating defects. In conventional FSW, the viscoplastic material flow originated by the rotating tool and the severe plastic deformation around it, may be insufficient to promote effective joining. The rotation to travel speed ratio (Ω/V) [rev/mm] can be increased to raise the heat input in conventional FSW, since it increases the viscoplastic material flow. However, this cannot be possible, since it may be out of the optimal parameters window of the FSW process, or it may promote a wider HAZ with a higher loss of weld properties. The reasoning behind the use of the hybrid FSW process with electrical current was to add additional external

heat to raise the material temperature, improving the viscoplasticity and the stirring effect, without changing the optimum cinematic Ω/V ratio.

NiTi-Al composites have been produced by ultrasonic additive manufacturing [17]. Friction stir processing was also used to disperse and embed NiTi particles into an Aluminium matrix [15]. However, there was no reported attempts on producing NiTi-Al composites using bulk NiTi as reinforcement material.

In this work, NiTi-Al composites were produced by FSW assisted by Joule effect in order to improve interfacial adhesion of the two materials and, thus, to obtain functional composites.

Concept and Simulation

The concept of FSW assisted by electrical current, was discussed in [16] for similar welding of Al alloys. A new simulation model was developed for the present case, in order to understand the distribution of both the electric current density and the temperature in the lap joint configuration consisting of Al-NiTi-Al. The developed model includes both analytical and numerical simulation.

The geometry of the model comprises the FSW tool, two plates of aluminium with a NiTi ribbon between these and the steel backing plate (Figure 1). The heat is generated by the Joule effect due to the electrical current that flows from the FSW tool, through the materials into the backing plate. To calculate the heat input, the model assume the same simplifying hypotheses described in [16].

The temperature increase due to Joule effect was estimated by the fundamental calorimetric equation (Eq. 1) which, in this particular case, corresponds to Eq. 2, where R [Ω] is the electrical resistance of the material, I [A] is the current intensity, t [s] is the time of the applied current, m [kg] is the mass dissipating heat, C_p [J/kg°C] is the specific heat of material and T [°C] is the increment in temperature. The electrical resistance can be calculated by Eq. 3, where h [m] is the height, ρ_e [Ω·m] is the electrical resistivity and ϕ [m] is the diameter of the control volume considered. The time of the applied current t [s] in the control volume is given by Eq. 4, were ϕ_{tool} [m] is the tool diameter and V_x [m/s] is the welding speed. The mass m [kg] was calculated according to Eq. 5, considering the material density ρ [kg/m^3], the height h [m] and diameter (ϕ) [m] of the control volume.

Substituting Eqs. 3 to 5 into Eq. 2 the increase of the temperature ΔT [ºC] can be computed by Eq. 6, were J [A/m^2] is the electric current density that flows through the materials.

From this equation, four factors were identified that directly contribute to the temperature increase, and these are related to: (i) material properties ($\rho_e/\rho(C_p)$); (ii) dimension of the FSW tool (φ); (iii) FSW travel speed (V_x); and (iv) electric current density (J).

$$Q_{Joule\ \ effect} = Q_{Increase\ \ temperature} \tag{1}$$

$$R \cdot I^2 \cdot t = m \cdot C_p \cdot \Delta T \tag{2}$$

$$R = \frac{h \cdot \rho_e}{\pi \cdot \frac{\phi^2}{4}} \tag{3}$$

$$t = \frac{\phi_{tool}}{V_x} \tag{4}$$

$$m = \rho \cdot h \cdot \pi \cdot \frac{\phi^2}{4} \tag{5}$$

$$\Delta T = \frac{\rho_e}{\rho \cdot C_p} \cdot \frac{\phi^2}{V_x} \cdot J^2 \tag{6}$$

CST-EM Studio Suit Student Edition was used for numerical simulation with Finite Element Method (FEM) in order to calculate the electric current density *J* [A/m^2] flowing through the materials. A mesh of about 30×10^3 hexahedral elements was used. The simulation comprised a current intensity of 900 A, which was forced to flow from the top of the tool to the base plate (Figure 2 a). As the electrical conductivity of the aluminium (35.6×10^6 S/m) is higher than that of NiTi (1.22×10^6 S/m), the current density is much higher in aluminium, as depicted in b).

The electrical current density was numerically calculated along six lines parallel to the back plate at distances of 1.5 to 10 mm from the base of the back plate. Figure 1 b) depicts these lines and their positioning by red dotted lines. Data from numerical calculation was introduced into Eq. 6 to determine analytically the temperature increase due to the Joule effect. As shown in Figure 3, this temperature increase is higher in the NiTi boundary (about 80 ºC), since this is the most electrical resistant material, while it is quite low both in the aluminium and in the backing plate. The increment of temperature in the FSW tool due the Joule effect is of about 40 ºC.

As a consequence, the temperature in both materials raise facilitating the viscoplastic behaviour of the aluminium matrix (Figure 2) promoting better joining of Al to NiTi.

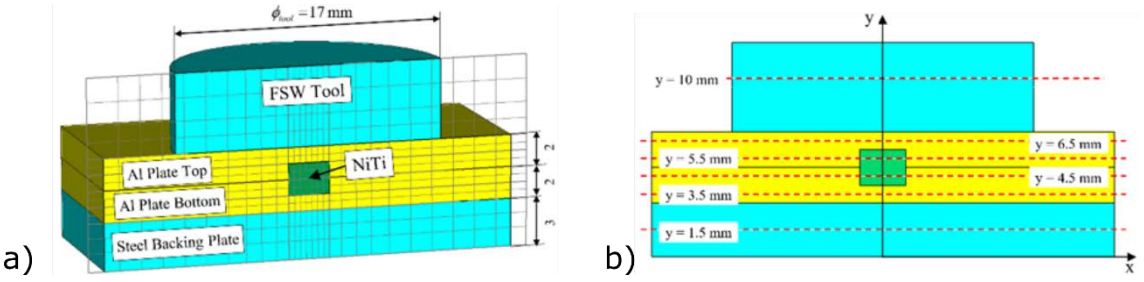

Figure 1 – Geometrical model of the FSW assisted by electrical current for production of Al/NiTi composites. a) General overview and mesh, b) positioning of the six horizontal dotted red lines were the electrical current density was numerically calculated.

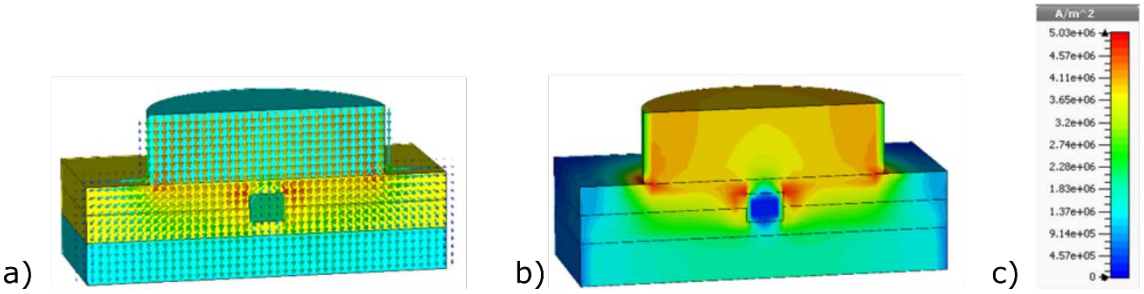

Figure 2 – Numerical simulation of the electrical current density distribution. a) Vector field representation; b) contour plot display in the transversal plane.

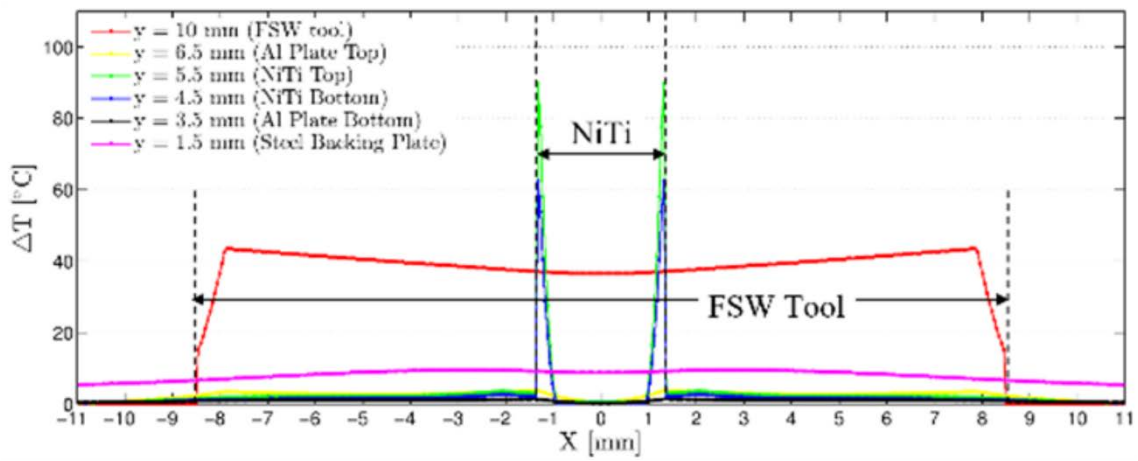

Figure 3 – Temperature increment due to Joule effect at different distances to the base of the back plate identified by red dotted lines in Figure 1 b).

Materials and Methods

Aluminium 1100 (AA1100) plates were used for the matrix, with 1.6 mm thick, 100 mm wide and 200 mm length. Ni-rich NiTi (51 at. %) ribbons, with a cross section of 2.8 × 0.9 mm^2 were used as reinforcements with the same length.

Prior to welding, both materials were mechanical and chemically cleaned to remove grease and oxides. NiTi was placed in between the two aluminium plates in a lap joint configuration. In order to guarantee a good positioning of NiTi ribbons, these were pre-placed between the Al plates and the "sandwich" was cold forged, so that plastic deformation of the Al could create a chamfer where NiTi could settle (Figure 4).

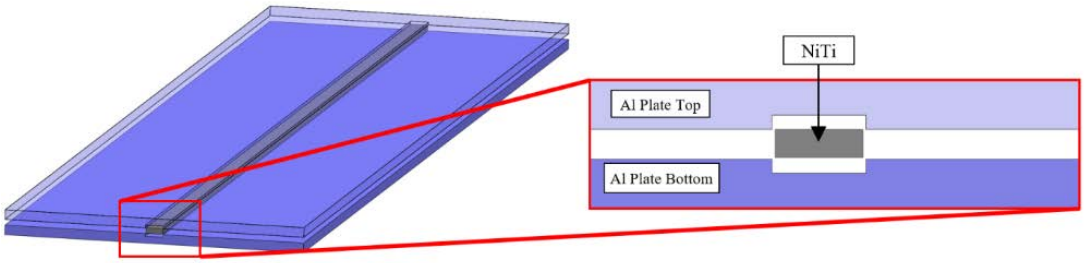

Figure 4 – Aluminium plates with NiTi ribbon and chamfer produced on one of the aluminium plates.

The friction stir welding tool used was selected so that it could conduct the electrical current with no interference with the machine electrical circuit and confine the current to the layer below the probe, in order to avoid the electrical current to flow freely through the tool main body and shoulder. The tool rotation and travel speed were set constant at 910 rev/min and 71 mm/min, respectively. Three weld beads were made in a sequence as depicted in Figure 5. Electrical current was introduced at a predefined position, corresponding to dashed line 2 in Figure 5, to promote local heating of the materials.

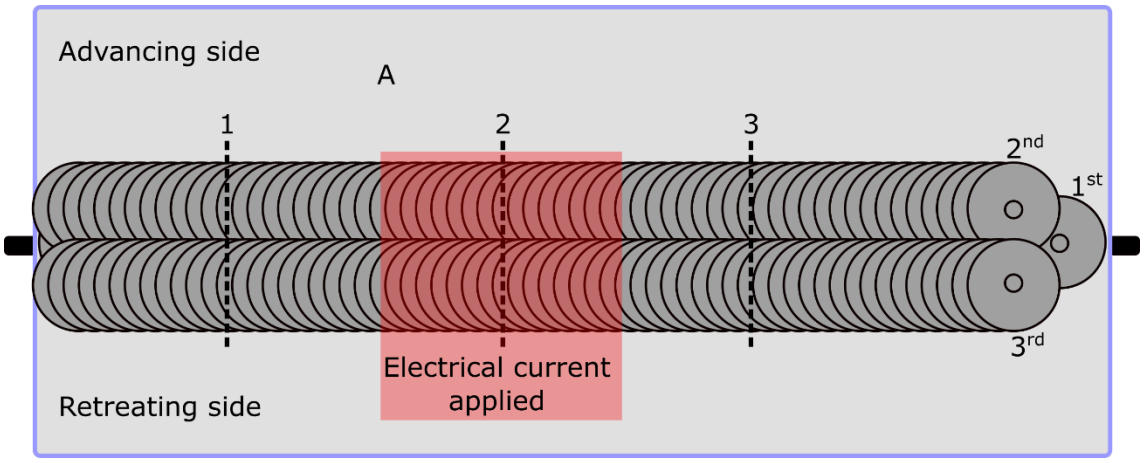

Figure 5 – Schematic representation of the obtained composites (not to scale).

During FSW, temperature variation was measured with three type-K thermocouples, placed as depicted in Figure 6, where T1, T2 and T3 correspond to the temperatures measured at positions 1, 2 and 3, respectively.

Each FSW pass started with no electrical current and this was introduced when traveling near position 2 (Figure 5). So, in the same pass, the effect of the electrical current could be assessed by analysing the processed material at the selected positions 1, 2 and 3 identified in Figure 5.

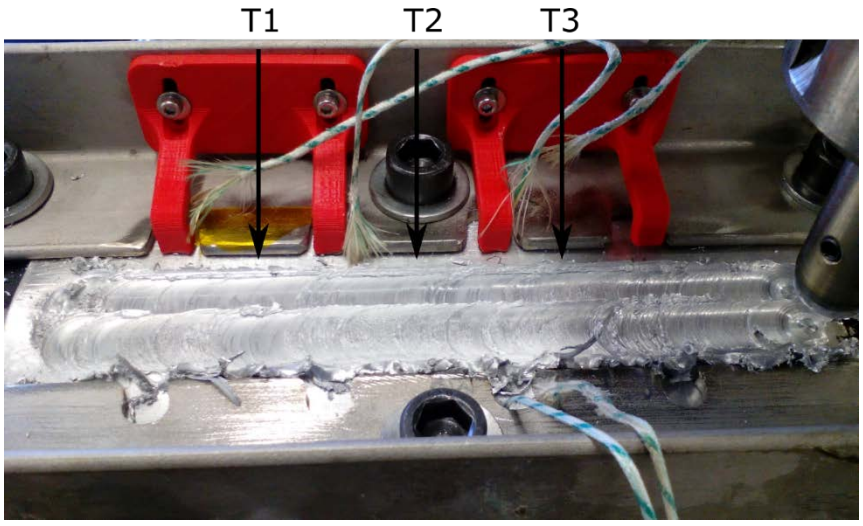

Figure 6 – Position of the thermocouples for determination of the temperatures during the welding process.

Cross sections at these positions were prepared for microstructural analysis by optical microscopy. Scanning electron microscopy, using a Zeiss DSM 962 ESM, was used to analyse the bonding characteristics at the contact interfaces between the two base materials.

For determination of the microstructural changes induced by the FSW assisted process, synchrotron X-ray diffraction was performed at the pre-defined positions of the welded joints. These measurements were carried out in beamline P07 High Energy Materials Science (HEMS) of Petra III/DESY. Working in transmission mode, the wavelength was set at 0.1426 Å (87 keV) and the sample to the 2D Mar345 detector was 1412 mm. The beam spot size was of 100 × 100 µm. The raw images were integrated along the azimuthal angle using Fit2D [18] to obtain the X-ray diffraction patterns of each region. This way it was possible to perform microstructural characterization of the existing phases in the distinct analysed regions [19].

Mechanical characterization of the friction stir welded composites consisted on bending tests up to 90^{o} using an Autograph Shimadzu AG50kNG tensile machine equipped with a 50 kN load cell. To evaluate the interfacial resistance between NiTi and aluminium, pull-out tests were also performed. In all mechanical testing the cross-head displacement speed was set at 2 mm/min.

Results and Discussion

FSW assisted by electrical current was effective to produce composites in a matrix of Al reinforced with NiTi ribbons.

The effect on the electrical current is clearly observed as shown in Figure 7 a) and b). In conventional FSW (Figure 7 a) a lack of joining along the Al/Al and Al/NiTi/Al interfaces is observed, while when the electrical current was used to assist the welding process, an effective joining was achieved (Figure 7 b). Due to the softening of the Al base material an increase in the visco-plastic material flow around the ribbon is observed, with almost complete bonding around it. Figure 7 a) clearly shows that the ribbon is not bonded to the matrix and the Al plates have an incipient bonding to each other, despite the fact that three passes have been performed in the NiTi region, as described previously. Additionally, in some cases, the force exerted by the tool was high and induced misalignments of the reinforcing ribbons.

Scanning electron microscopy at the Al/NiTi interface in both assisted and non-assisted friction stir welded joints was carried out and is shown in Figure 8. From this figure it can be observed that when no electrical current is used, joining along the Al/NiTi interface occurs at limited locations where bridging of both materials can be seen. On the other hand, in FSW assisted by electrical current, bonding between the matrix and the reinforcements is much more continuous. Both optical and scanning electron microscopy observations emphasize the significant influence of the electrical current, facilitating joining between Al and NiTi and impregnating NiTi with Al.

a)

b)

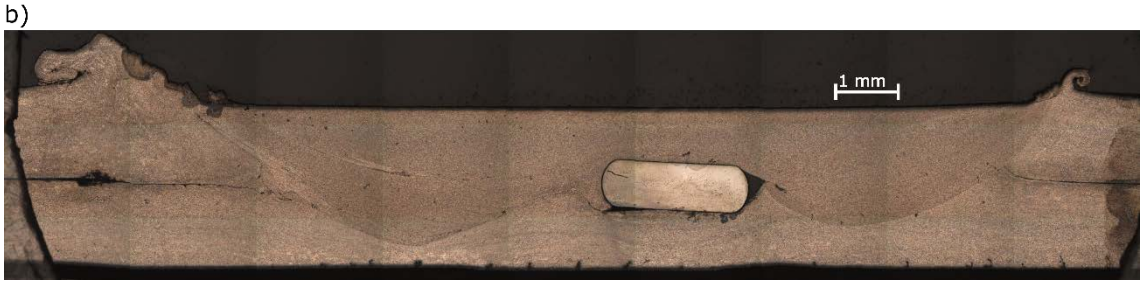

Figure 7 – Optical microscopy of an Al/NiTi joint produced without electrical current (a) and with an electrical current intensity of 900 A (b).

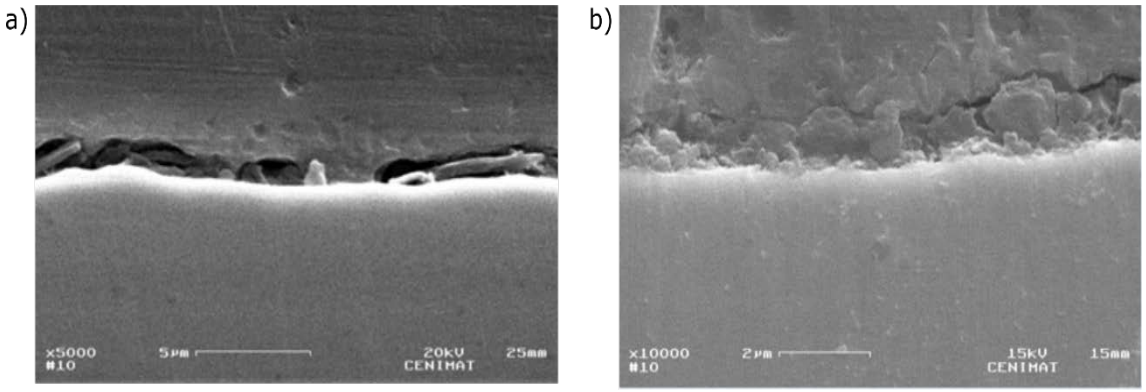

Figure 8 – Scanning electron microscopy of the Al/NiTi interface of a friction stir welded joint: a) produced without electrical current; b) assisted by electrical current.

In order to assess whether the process affected the NiTi microstructure, X-ray diffraction analysis using synchrotron radiation was performed in three distinct regions (dashed lines 1, 2 and 3 in Figure 5). It can be observed that in the welded region, position 1, before the insertion of the electrical current, Al_2O_3, Al and NiTi austenite were identified (Figure 9 a). However, at the regions where the electrical current was inserted and, even after it was removed, a peak of NiTi martensite was observed (Figure 9 b and c).

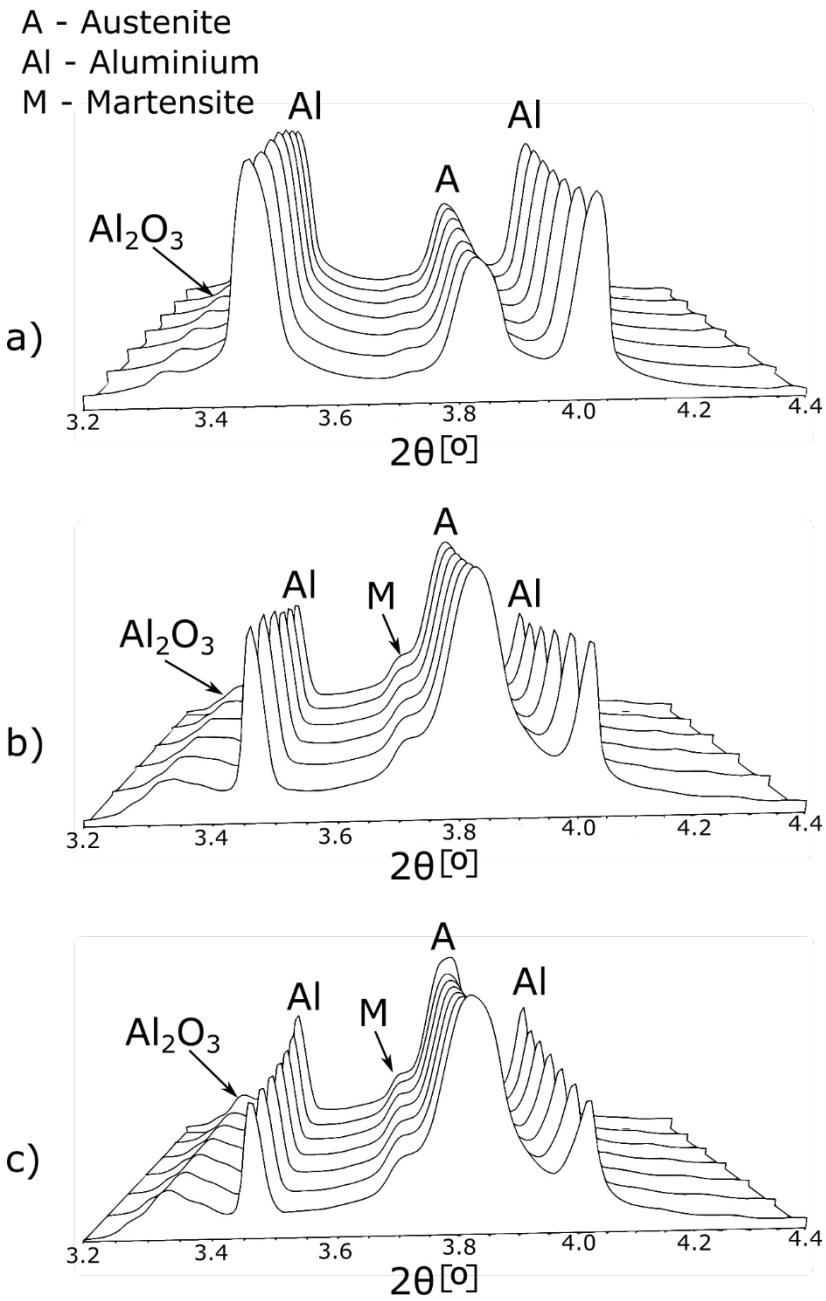

Figure 9 – X-ray diffraction patterns in different regions of the welded material: a) before the insertion of the electrical current; b) at the insertion of electrical current; c) after insertion of electrical current. a), b) and c) correspond to the dashed lines 1, 2 and 3 of Figure 5, respectively.

Previously, it was observed that fully austenitic NiTi can show some martensite in the heat affected zone of laser welded NiTi joints [20,21]. The reason for the observation at room temperature of martensite after welding, was attributed to Ni_4Ti_3 precipitation, which can occur in a temperature range between 350 and 500 °C according to the TTT diagrams available for these alloys [22,23]. As a consequence of these Ni-rich precipitates, the transformation temperatures of NiTi raised, thus allowing for martensite to be stable at room temperature [8,24]. It was also noticed that even for short lapses of time, within the few seconds, Ni_4Ti_3 precipitation could occur, thus explaining the microstructural changes observed in the thermally affected regions of the joints. However, it must be noticed that the formation of martensite at room temperature may not be detrimental to the overall mechanical behaviour of the "sandwich". Due to the hysteretic movement of the interfaces (martensite variant

interfaces, twin boundaries) [25] the damping capacity of the produced composite can be improved.

In fact, from the temperature evolution measurements obtained during electrical assisted FSW (Figure 10) it can be seen that in the region immediately before the insertion of electrical current, a maximum temperature of nearly 175 °C was measured. Significant improvement was observed as the weld proceeds for two different reasons: as the tool advanced more heat is generated due to tool wear and bulk material plastic deformation, allowing for a raise in temperature; this temperature raise is complemented by the insertion of electrical current during the process. While T2 curve was measured near the region where the electrical current was introduced, T3 was measured after this point. For this reason, a minor temperature decrease is observed. Nonetheless, it is clear that both regions experienced temperatures between 350 and 500 °C for a few seconds, which was enough to enable Ni_4Ti_3 precipitation as reported by [21].

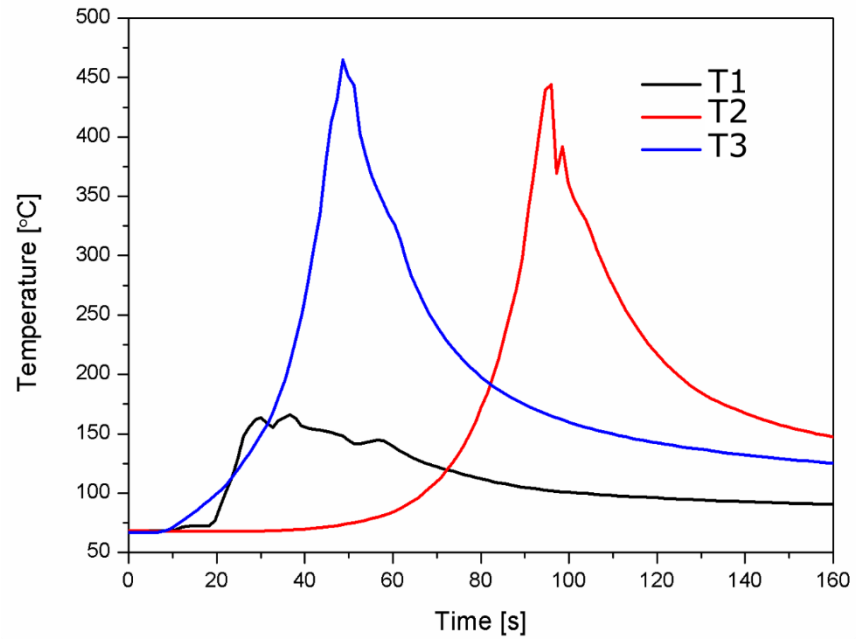

Figure 10 – Temperature profile at different regions of the welded joint.

Bending tests were performed on the welded joints produced with and without electrical current (Figure 11). A significant improvement of the joint strength was achieved when the electrical current was applied simultaneously with friction stir welding: the maximum strength of the FSW without electrical current was of about 80 MPa and increased to nearly 135 MPa with the hybrid process. This is related to the fact that a longer joining interface (Al/Al and Al/NiTi/Al) was obtained and, thus, the strength increased. It is expected that, if full joining between NiTi and Al is achieved the strength can increase even further. It is worth mentioning that in both cases, with and without electrical current, all samples were bent up to 90^o angle without fracture (Figure 12).

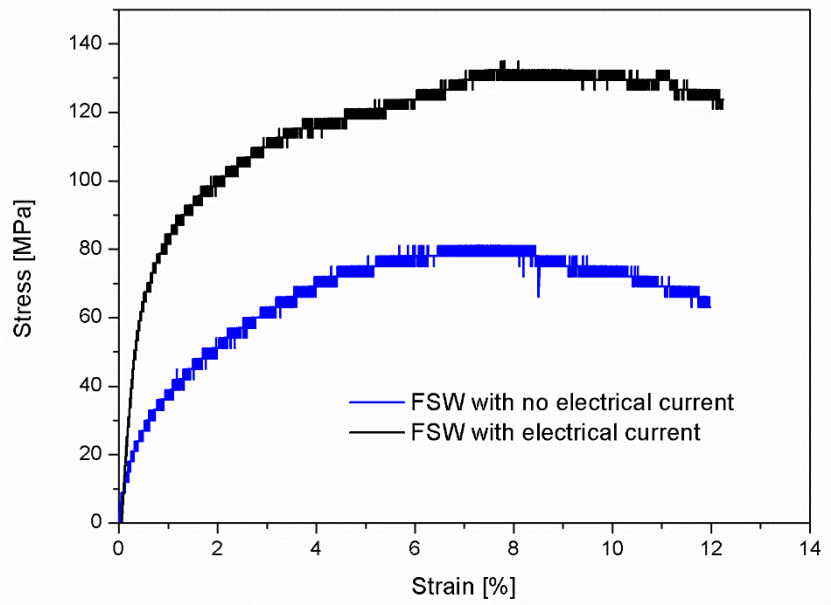

Figure 11 – Bending tests performed on Al/NiTi friction stir welded joints produced with and without electrical current.

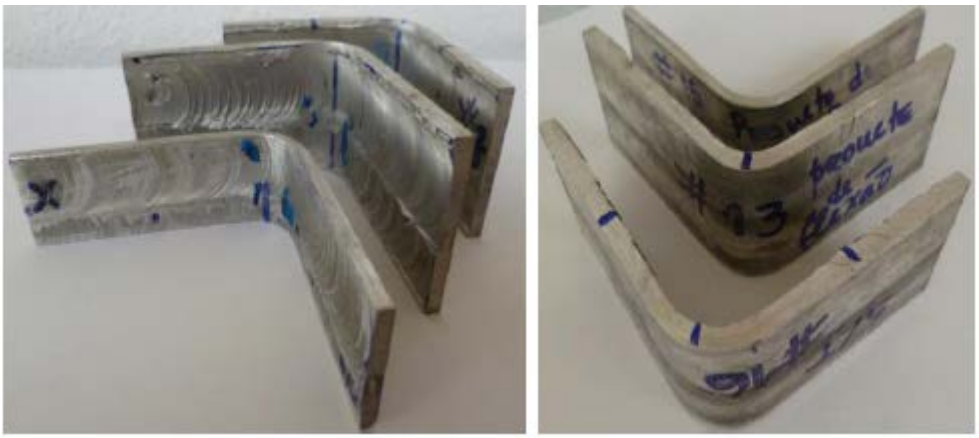

Figure 12 – Specimens after bending tests: a) with electrical current; b) without electrical current.

Pull-out tests were also carried out to analyse the interfacial strength in both types of joints (Figure 13). The shear strength of the composite produced with electrical current is significantly higher than when no electrical current is used (13.6 MPa vs 8.8 MPa). Hahnlen et al. [17] computed that the shear strength exhibited by the NiTi-Al interface in a composite produced by ultrasonic additive manufacturing was nearly 7 MPa. Thus, using FSW hybrid process, the shear strength doubles, which is a remarkable result despite the fact that some regions of the NiTi ribbon were not completely bonded to the aluminium matrix.

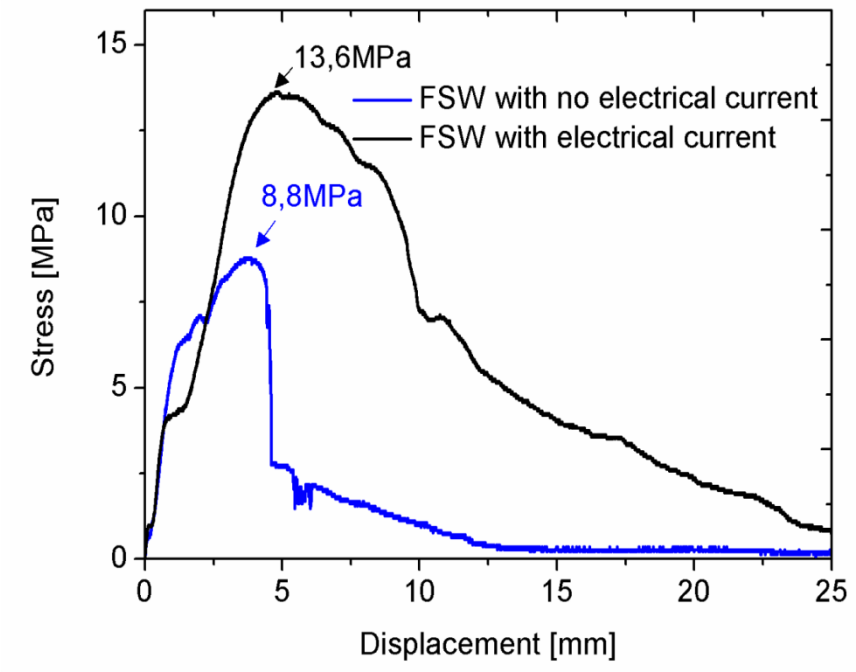

Figure 13 – Pull-out tests performed on the welded joints.

Conclusions

From the work conducted the following conclusions can be drawn:

- Friction stir welding assisted by electrical current was used to produce Al/NiTi/Al composites.

- The insertion of electrical current increased the visco-plastic material flow due to the temperature increase, which was calculated to be of about 80 ºC in the interface AA-NiTi, allowing a better bonding of NiTi ribbons to the aluminium matrix.

- As a result of the increased temperatures experienced during the welding process, the originally fully austenitic NiTi base material, presented evidence of both austenite and martensite at room temperature. This martensite was formed as a consequence of the raise in the transformation temperatures of NiTi which occurred due to precipitation phenomena during welding.

- Bending tests showed a greater tensile strength when the composites were produced by FSW assisted with electrical current, compared to those manufactured by FSW (135 MPa *vs.* 80 MPa).

- The interfacial strength of the joints produced with electrical current is considerably higher than those produced with no electrical current (13.6 MPa vs 8.8 MPa). This occurs due to better bonding between Al and NiTi as a result of the higher temperatures achieved during the process and, thus, the improved material viscoplasticity.

Acknowledgements

The authors would like to acknowledge Fundação para a Ciência e Tecnologia (FCT) for its financial support via the project PEst-OE/EME/UI0667/2014. TS and RM acknowledge Project Hi2TRUST, (Refª 3335), supported by Fundo Europeu de Desenvolvimento Regional (FEDER), Programa Operacional Regional de Lisboa (Lisb@2020 and Portugal2020). JPO acknowledges funding of CENIMAT/i3N by FEDER funds through the COMPETE 2020 Programme and National

Funds through FCT — Portuguese Foundation for Science and Technology under the project UID/CTM/50025/2013.

References

[1] T. Dursun, C. Soutis, Recent developments in advanced aircraft aluminium alloys, Mater. Des. 56 (2014) 862–871. doi:10.1016/j.matdes.2013.12.002.

[2] J. Zhang, Y. Liu, Y. Huan, S. Hao, D. Jiang, Y. Ren, et al., High damping NiTi/Ti3Sn in situ composite with transformation-mediated plasticity, Mater. Des. 63 (2014) 460–463. doi:10.1016/j.matdes.2014.05.062.

[3] M.F. Ashby, Y.J.M. Bréchet, Designing hybrid materials, Acta Mater. 51 (2003) 5801–5821. doi:10.1016/S1359-6454(03)00441-5.

[4] I. Schmidt, R. Lammering, The damping behaviour of superelastic NiTi components, Mater. Sci. Eng. A. 378 (2004) 70–75. doi:10.1016/j.msea.2003.09.106.

[5] E. Graesser, F. Cozzarelli, Shape-Memory Alloys as New Materials for Aseismic Isolation, J. Eng. Mech. 117 (1991) 2590–2608. doi:10.1061/(ASCE)0733-9399(1991)117:11(2590).

[6] S. Nemat-Nasser, W.G. Guo, Superelastic and cyclic response of NiTi SMA at various strain rates and temperatures, Mech. Mater. 38 (2006) 463–474. doi:10.1016/j.mechmat.2005.07.004.

[7] K. Wada, Y. Liu, Shape recovery of NiTi shape memory alloy under various pre-strain and constraint conditions, Smart Mater. Struct. 14 (2005) S273–S286. doi:10.1088/0964-1726/14/5/016.

[8] K. Otsuka, X. Ren, Physical metallurgy of Ti-Ni-based shape memory alloys, Prog. Mater. Sci. 50 (2005) 511–678. doi:DOI 10.1016/j.pmatsci.2004.10.001.

[9] J.P. Oliveira, R.M. Miranda, F.M. Braz Fernandes, High Strain and Long Duration Cycling Behavior of Laser Welded NiTi Sheets, Int. J. Fatigue. 83 (2015) 195–200. doi:10.1016/j.ijfatigue.2015.10.013.

[10] D. Yang, H.C. Jiang, M.J. Zhao, L.J. Rong, Microstructure and mechanical behaviors of electron beam welded NiTi shape memory alloys, Mater. Des. 57 (2014) 21–25. doi:10.1016/j.matdes.2013.12.039.

[11] J.P. Oliveira, B. Panton, Z. Zeng, C.M. Andrei, Y. Zhou, R.M. Miranda, et al., Laser joining of NiTi to Ti6Al4V using a Niobium interlayer, Acta Mater. 105 (2016) 9–15. doi:10.1016/j.actamat.2015.12.021.

[12] A. Shojaei Zoeram, S.A.A. Akbari Mousavi, Laser welding of Ti–6Al–4V to Nitinol, Mater. Des. 61 (2014) 185–190. doi:10.1016/j.matdes.2014.04.078.

[13] R. Nandan, T. DebRoy, H.K.D.H. Bhadeshia, Recent advances in friction-stir welding - Process, weldment structure and properties, Prog. Mater. Sci. 53 (2008) 980–1023. doi:10.1016/j.pmatsci.2008.05.001.

[14] O.S. Salih, H. Ou, W. Sun, D.G. McCartney, A review of friction stir welding of aluminium matrix composites, Mater. Des. 86 (2015) 61–71. doi:10.1016/j.matdes.2015.07.071.

[15] M. Dixit, J.W. Newkirk, R.S. Mishra, Properties of friction stir-processed Al 1100–NiTi composite, Scr. Mater. 56 (2007) 541–544. doi:10.1016/j.scriptamat.2006.11.006.

[16] T.G. Santos, R.M. Miranda, P. Vilaça, Friction Stir Welding assisted by electrical Joule effect, J. Mater. Process. Technol. 214 (2014) 2127–2133. doi:10.1016/j.jmatprotec.2014.03.012.

[17] R. Hahnlen, M.J. Dapino, NiTi–Al interface strength in ultrasonic additive manufacturing composites, Compos. Part B Eng. 59 (2014) 101–108. doi:10.1016/j.compositesb.2013.10.024.

[18] A.P. Hammersley, S.O. Svensson, M. Hanfland, A.N. Fitch, D. Hausermann, Two-dimensional detector software: From real detector to idealised image or two-theta scan, High Press. Res. 14 (1996) 235–248. doi:10.1080/08957959608201408.

[19] J.P. Oliveira, F.M.B. Fernandes, R.M. Miranda, N. Schell, J.L. Ocaña, Residual stress analysis in laser welded NiTi sheets using synchrotron X-ray diffraction, Mater. Des. 100 (2016) 180–187. doi:10.1016/j.matdes.2016.03.137.

[20] J.P. Oliveira, F.M.B. Fernandes, N. Schell, R.M. Miranda, Martensite stabilization during superelastic cycling of laser welded NiTi plates, Mater. Lett. 171 (2016) 273–276. doi:10.1016/j.matlet.2016.02.107.

[21] J.P. Oliveira, F.M. Braz Fernandes, R.M. Miranda, N. Schell, On the Mechanisms for Martensite Formation in YAG Laser Welded Austenitic NiTi, Shape Mem. Superelasticity. 2 (2016) 114–120. doi:10.1007/s40830-016-0058-z.

[22] M. Nishida, C.M. Wayman, T. Honma, Precipitation processes in near-equiatomic TiNi shape memory alloys, Metall. Trans. A. 17 (1986) 1505–1515. doi:10.1007/BF02650086.

[23] A.R. Pelton, J. Dicello, S. Miyazaki, Optimisation of processing and properties of medical grade Nitinol wire, Minim. Invasive Ther. Allied Technol. 9 (2000) 107–118. doi:10.3109/13645700009063057.

[24] K. Gall, H. Sehitoglu, Y.I. Chumlyakov, I. V. Kireeva, H.J. Maier, The Influence of Aging on Critical Transformation Stress Levels and Martensite Start Temperatures in NiTi: Part II—Discussion of Experimental Results, J. Eng. Mater. Technol. 121 (1999) 28. doi:10.1115/1.2815995.

[25] J. Van Humbeeck, Damping capacity of thermoelastic martensite in shape memory alloys, J. Alloys Compd. 355 (2003) 58–64. doi:10.1016/S0925-8388(03)00268-8.